Development of Enhanced Seismic Compactness Requirements for Webs in Wide-Flange Steel Columns

Gulen Ozkula[1]; Chia-Ming Uang, M.ASCE[2]; and John Harris, M.ASCE[3]

Abstract: Recent full-scale testing of steel wide-flange columns under axial compression and cyclic lateral drifts for special moment frame applications showed that deep, slender columns could experience significant flexural strength degradation due to plastic hinge formation with buckling modes and considerable axial shortening within the hinge. Test results showed that the interaction between web and flange local buckling played a significant role for the observed degradation, even when the cross-sectional elements met the highly ductile limiting width-to-thickness ratios specified in the current seismic design standard for steel frames. These observations were also confirmed by numerical simulations. Enhanced limiting width-to-thickness ratios for the web of a wide-flange column for both special and intermediate steel moment frames are proposed to limit the severity of strength degradation and axial shortening. **DOI: 10.1061/(ASCE)ST.1943-541X.0003036.** © *2021 American Society of Civil Engineers.*

Author keywords: Seismic design; Steel moment frames; Wide-flange columns; Buckling; Width-thickness ratios.

Introduction

The steel special moment frame (SMF) composed of wide-flange beams and columns is a popular seismic force-resisting system (SFRS) in high seismic regions in the United States. Prior to the Northridge, California, earthquake in 1994, shallow W12 or W14 columns [nominal depth = 305 mm (12 in.) or 356 mm (14 in.), respectively] were commonly used. Since 1994, designers have increasingly used deeper column sections [e.g., W24, nominal depth = 610 mm (24 in.) and deeper] to increase the lateral frame stiffness to meet the stringent story drift requirements specified in modern building codes.

Lateral stiffness of an SMF is a function of the moment of inertias of the frame beams and columns. For SMF design with wide-flange sections, the width-to-thickness ratios of the flanges ($\lambda_f = b_f/2t_f$, where b_f = flange width and t_f = flange thickness) and web ($\lambda_w = h/t_w$, where h = web height and t_w = web thickness) cannot exceed the "highly ductile" limiting ratios, λ_{hd}, specified in AISC 341-16 (AISC 2016b). For intermediate moment frame (IMF) design, the width-to-thickness ratios cannot exceed the "moderately ductile" limiting ratios, λ_{md}. These limiting ratios set the requirement for seismic compactness of the cross-section elements; see Table 1 for these seismic compactness values, where C_a is defined as follows:

$$C_a = \frac{P_u}{\phi_c R_y A_g F_y} \tag{1}$$

where P_u = applied axial force; A_g = cross-sectional area; F_y = specified minimum yield stress; R_y = ratio of the expected yield stress to F_y; and $\phi_c = 0.9$.

Prior to the Northridge, California, earthquake, research on steel moment frames in the United States focused mainly on the moment connection between wide-flange beams and wide-flange columns (beam-to-column connection), especially the welded flange-bolted web connection. Following the growing trend to provide a strong-column weak-beam design, SMF columns (except for the panel zones and column bases) were expected to remain elastic. Reduced-scale column sizes used for cyclic testing were relatively shallow and axial loads were not commonly applied to the columns in beam-to-column connection tests because of the difficulty of applying the load cyclically in the laboratory. Popov et al. (1975) applied axial loads to the column in a beam-to-column subassembly test, where four shallow column sections (W8 × 28 and W8 × 48) oriented for strong-axis bending were tested. The applied axial load remained constant and the axial load ratio (P/P_y, where $P_y = A_g F_y$ = nominal yield strength of column) for each test was set between 0.3 and 0.8. The study concluded that the axial load ratio should be kept below 0.5 because a sharp drop in lateral strength was observed at a higher axial force ratio. This degradation was precipitated by flange local buckling with a significant amount of axial shortening within the plastic hinge zone. FEMA 273 (FEMA 1997) adopted this limit to distinguish between force-controlled and deformation-controlled column sections and it was maintained until ASCE 41-17 (ASCE 2017).

Eight reduced-scale isolated wide-flange columns were tested by MacRae (1990); values for λ_f and λ_w were 8.94 and 25.0, respectively. The column length was relatively short, with a member slenderness ratio, $\lambda_L = L/r_y$ (where L = member length and r_y = radius of gyration about weak-axis), of 17 so that flexural buckling was unlikely. The applied axial load ranged from 0.0 to $0.8P_y$. Significant axial shortening within the plastic hinge zone due to local buckling of the cross-sectional elements was reported. Pseudodynamic testing of five first-story beam-to-column subassemblies was conducted by Schneider et al. (1993); the specimens were subjected to both axial compression and lateral drift. Two column sections were investigated (W10 × 30 and W12 × 26). For the W column

[1]Assistant Professor, Dept. of Civil Engineering, Tekirdağ Namik Kemal Univ., Tekirdağ 59860, Turkey. Email: gozkula@nku.edu.tr

[2]Professor, Dept. of Structural Engineering, Univ. of California, San Diego, La Jolla, CA 92093 (corresponding author). ORCID: https://orcid.org/0000-0002-8467-9748. Email: cmu@ucsd.edu

[3]Research Structural Engineer, National Institute of Standards and Technology, Gaithersburg, MD 20899. Email: john.harris@nist.gov

Note. This manuscript was submitted on February 27, 2020; approved on February 3, 2021; published online on April 29, 2021. Discussion period open until September 29, 2021; separate discussions must be submitted for individual papers. This paper is part of the ***Journal of Structural Engineering***, © ASCE, ISSN 0733-9445.

Table 1. Limiting width-to-thickness ratios for wide-flange columns per AISC 314-16

Limiting λ	Flange	Web
λ_{hd} for highly ductile members	$0.32\sqrt{E/(R_yF_y)}$	When $C_a > 0.114$: $0.88\sqrt{E/(R_yF_y)}(2.68 - C_a) \geq 1.57\sqrt{E/(R_yF_y)}$ When $C_a \leq 0.114$: $2.57\sqrt{E/(R_yF_y)}(1 - 1.04C_a)$
λ_{md} for moderately ductile members	$0.40\sqrt{E/(R_yF_y)}$	When $C_a > 0.114$ $1.29\sqrt{E/(R_yF_y)}(2.12 - C_a) \geq 1.57\sqrt{E/(R_yF_y)}$ When $C_a \leq 0.114$: $3.96\sqrt{E/(R_yF_y)}(1 - 3.04C_a)$

Note: E = modulus of elasticity; and C_a is defined in Eq. (1).

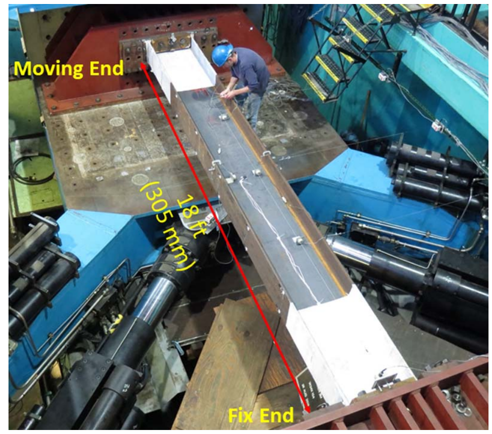

Fig. 1. Test setup.

($\lambda_f = 5.7$ and $\lambda_w = 29.5$), minor local buckling was observed. However, significant local buckling at the column base was observed for the more slender W column ($\lambda_f = 8.5$ and $\lambda_w = 47.2$).

After the Northridge earthquake, a significant number of full-scale beam-to-column moment connections were tested after brittle weld fracture in welded flange-bolted web connections in moment frame buildings. A large FEMA-funded study was conducted by the SAC Joint Venture (FEMA 2000). The focus of that study was on beam-to-column connections to ensure that plastic hinging in frame beams would occur while protecting the connection welds from brittle fracture. The majority of the connection tests conducted considered shallow (W12 or W14) columns to reflect design practice at that time. Chi and Uang (2006) supplemented the FEMA study by cyclically testing three full-scale exterior beam-to-column connections using beams with a reduced beam section (RBS) and W27 column sections. Although no axial loads were applied to the column, twisting of the columns was observed in all three tests—a phenomenon not previously reported in similar tests using more shallow column sections. It was found that the twisting was caused by an eccentric beam flange force being applied to the column flange due to lateral-torsional buckling of the beam. This testing is understood to be the first time that the concern of "deep column" behavior was observed.

Newell and Uang (2008) conducted tests on isolated wide-flange shallow column sections under cyclic axial load and lateral drift. Shallow columns are widely used in braced frames because axial strength, not lateral stiffness, commonly dictates the section size. During an earthquake, these columns can be subjected to a high cyclic axial force combined with inelastic rotation demand resulting from lateral story drift once brace strength degrades. Cyclic testing of nine full-scale W14 columns (W14 × 132 to W14 × 370) representing a practical range of flange and web width-to-thickness ratios were subjected to different levels of axial force demand (0.35, 0.55, and $0.75P_y$) combined with up to a story drift angle of 0.1 rad. Flange local buckling was the dominant buckling mode, and no global buckling was observed in any test. Specimens achieved story drift capacities of 0.07–0.09 rad. These large deformation capacities were, in part, achieved due to the delay in flange local buckling resulting from the stabilizing effect provided by the stocky web (λ_w ranged from 6.9 to 17.7). In parallel, Newell and Uang (2006) demonstrated through finite element simulation that the cyclic behavior of deep columns (W27 × 146, W27 × 194, and W27 × 281) can be characterized by a rapid flexural strength degradation due to significant flange and web buckling.

To address the knowledge gap with deep, slender columns, the National Institute of Standards and Technology (NIST) developed a comprehensive research plan to study these columns at the member, subassemblage, and system levels (NIST 2011). Research at the member level, which started in 2013, was conducted at the University of California, San Diego (UCSD). In parallel, research on deep column sections was conducted by others. Researchers at the University of Michigan performed extensive finite element simulations to investigate deep column sections (Fogarty and El-Tawil 2015; Fogarty et al. 2017); λ_{hd} limiting values for both exterior and interior columns have been proposed (Wu et al. 2018). Both numerical simulations and testing of deep columns have also been conducted by Elkady and Lignos (2012, 2015, 2018), and Cravero et al. (2020), among others. The effect of column base flexibility on the cyclic response of first-story columns was also investigated through finite element simulation by Inamasu et al. (2019). Zargar et al. (2014) tested six 1/8-scale models of a W36 × 652 column ($\lambda_w = 16.3$ and $\lambda_f = 2.5$) with a scaled length of 493 mm (20 in.) ($\lambda_L = L/r_y = 38$). Both lateral drift and end rotation were applied at the top of the column specimen. Lateral-torsional buckling was the dominant failure mode observed for all specimens. Although notionally deep columns were tested (a prototype W36), it will be shown later that this section did not have the general characteristics of a deep column because the width-to-thickness ratios were extremely small.

Test Program

For the NIST research program, 48 full-scale deep column tests were conducted using a shake table test facility at UCSD (Ozkula and Uang 2015; Chansuk et al. 2018); Fig. 1 shows the test setup. Hot-rolled W30, W24, W18, and W14 sections of ASTM A992 (ASTM 2015) steel were selected, which covered a wide range of width-to-thickness ratios for the flanges and web. Table 2 shows some of the specimens that were tested. The distribution of the width-to-thickness ratios as well as the λ_{hd} and λ_{md} limits are depicted in Fig. 2. The member length was 5,486 mm (18 ft). Three levels of axial compression force were considered: $C_a = 0.2$, 0.4, and 0.6, with C_a defined per AISC 341-10 (AISC 2010) as follows:

$$C_a = \frac{P_u}{\phi_c A_g F_y} \tag{2}$$

Note that the above definition is slightly different from that in Eq. (1). Eq. (2) was used for C_a in Table 2, as this test program started before AISC 341-16 (AISC 2016b) was published in 2016.

Table 2. Test matrix

Group no.	Shape	Specimen no.	F_{ya}[a] (MPa) Flange	Web	Slenderness ratios λ_f	λ_w	λ_L	Axial load C_a[b]	P_u/P_y	Buckling mode[c]
1	W24 × 176	1L	362	404	4.81	28.7	71.1	0.2	0.18	CB
		1M						0.4	0.36	
		1H						0.6	0.54	
2	W24 × 131	2L	350	382	6.70	35.6	72.7	0.2	0.18	ALB
		2M						0.4	0.36	
		2M-NF						0.4	0.36	
		2H						0.6	0.54	
3	W24 × 104	3L	355	400	8.50	43.1	74.2	0.2	0.18	
		3M						0.4	0.36	
		3H						0.6	0.54	
4	W24 × 84	4L	353	405	5.86	45.9	110.8	0.2	0.18	CB
		4M						0.4	0.36	
12	W30 × 261	12LM	376	411	4.59	28.7	61.2	0.3	0.27	CB
13	W30 × 173	13M	395	463	7.04	40.8	63.2	0.4	0.36	ALB
		13M-BC								
14	W30 × 90	14L	402	432	8.52	57.5	103.4	0.2	0.18	
15	W18 × 192	15L	381	419	3.27	16.7	77.4	0.2	0.18	CB
16	W18 × 130	16M	344	367	4.65	23.9	80.0	0.4	0.36	
		16M-BC	359	390						
17	W18 × 76	17L	395	378	8.11	37.8	82.8	0.4	0.36	ALB
21	W18 × 130	21M-NF	378	407	4.65	23.9	80.0	0.4	0.36	CB
22	W30 × 148	22L	376	456	4.44	41.6	94.7	0.2	0.18	
23	W18 × 60	23L	340	382	5.44	38.7	100.0	0.2	0.18	
24	W14 × 82	24L	356	375	5.92	22.4	67.7	0.2	0.18	ALB
25	W14 × 53	25L	378	431	6.11	30.9	87.5	0.2	0.18	CB
26	W14 × 132	26LM	355	345	7.15	17.7	44.7	0.3	0.27	SFB

[a]Yield stress from tensile coupon testing.
[b]C_a is defined in Eq. (2).
[c]ALB = antisymmetric local buckling; CB = coupled buckling; and SFB = symmetric flange local buckling.

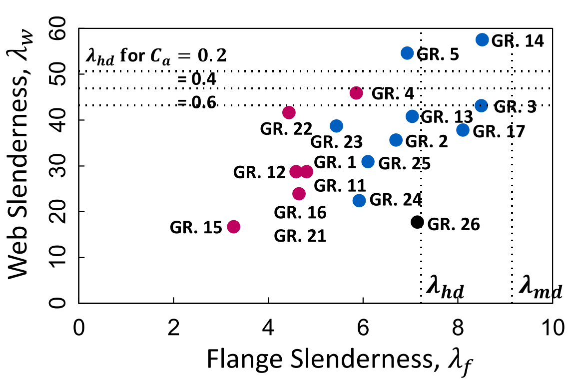

Fig. 2. Width-to-thickness ratio distribution.

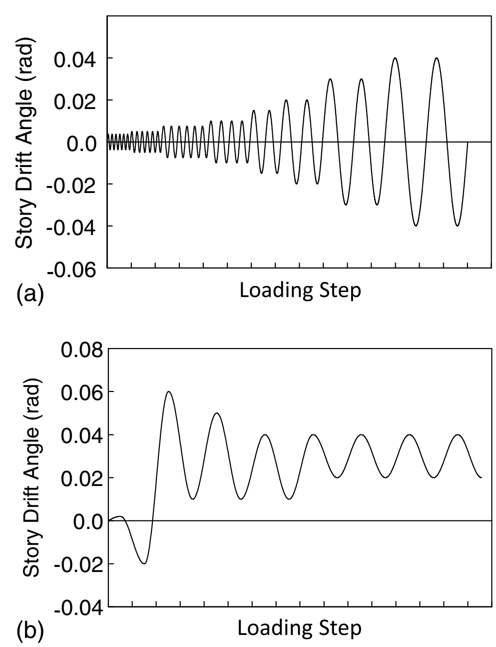

Fig. 3. Lateral loading sequence: (a) AISC loading sequence; and (b) SAC near-fault loading sequence.

In this work, constant and cyclic axial loads were used to simulate the axial demand for interior and exterior columns in an SMF, respectively. A fixed-fixed boundary condition was used for most of the specimens, with some specimens tested with a fixed-rotating boundary condition to simulate the end flexibility at the top of a first-story column. The cyclic story drift loading sequence specified in AISC 341 for prequalified beam-to-column moment connection testing was used for the majority of specimens [Fig. 3(a)]. A few specimens were tested with either the SAC near-fault loading protocol [Fig. 3(b)] (Krawinkler et al. 2000) or a monotonic pushover-type loading.

Under cyclic lateral loading, a beam-column, a column subjected to both axial and bending forces, can fail in one of three buckling modes (Ozkula et al. 2017). Fig. 4(a) shows a symmetrical flange buckling (SFB) mode in a W14 × 176 column when, due to the presence of a stocky web, each flange buckled locally in a symmetric mode with respect to the plane of the web (Newell and Uang 2008). The stocky web either did not buckle or experienced

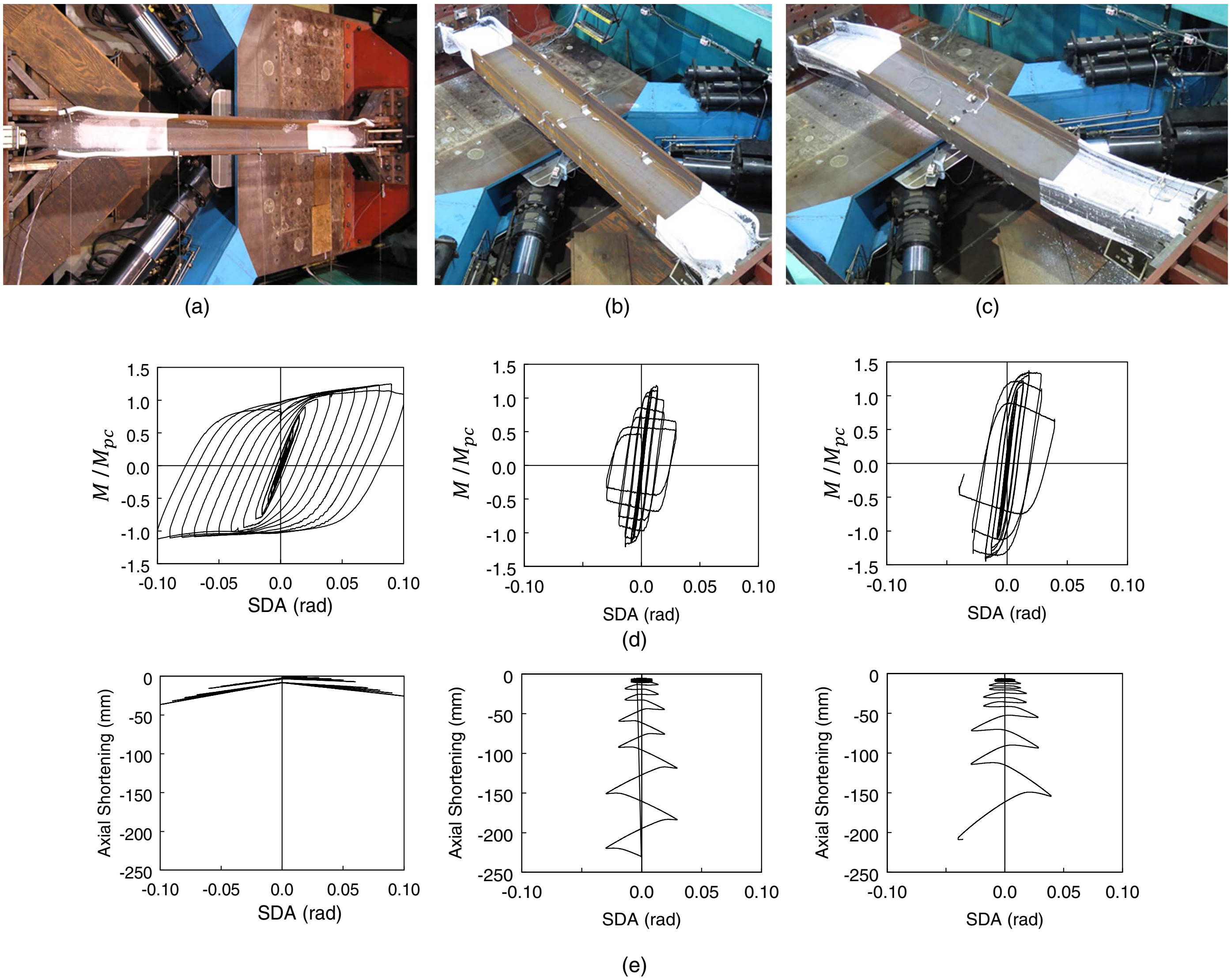

Fig. 4. Column cyclic behavior: (a) symmetric flange buckling; (b) antisymmetric local buckling; (c) coupled buckling; (d) normalized moment vs. SDA; and (e) axial shortening and SDA.

limited buckling. The other two buckling modes are typical of deep columns. An antisymmetric local buckling (ALB) mode in W24 × 131 column is shown in Fig. 4(b) and is characterized by an interaction between flange and web local buckling within the plastic hinge region. The column experienced a significant amount of axial shortening [Fig. 4(e)] and flexural strength degradation [Fig. 4(d)]. The third mode is a coupled buckling (CB) mode, shown in a W24 × 176 column in Fig. 4(c), which illustrated local buckling coupled with lateral-torsional buckling. This buckling mode also triggered significant axial shortening and strength degradation. The observed buckling mode for each specimen is listed in the last column of Table 2.

Finite Element Simulation

Finite element models of the test specimens were created in ABAQUS version 6.14 and then calibrated to match test data. The general-purpose shell element type (S4R) was used to model the specimens. This quadrilateral, doubly curved shell element could simulate large-deformation local buckling of the cross section and global buckling of the specimen. A sensitivity study showed that a mesh size of 25 mm (1 in.) was sufficient for modeling the specimens. Translation and rotation in all three directions was constrained at both ends of the model to simulate the fixed–fixed boundary conditions used in the tests [Fig. 5(a)]. A constant axial load was first applied before cyclic drifts were imposed to one end of the model. The model comprised the Von Mises yield surface, an associated flow rule, and a hardening law that included both nonlinear isotropic and kinematic hardening components, derived from cyclic coupon tests. Geometric imperfections were introduced in the model by superimposing buckling mode shapes obtained from an eigenvalue analysis. An out-of-plumbness of 1/500 represents the maximum tolerance on column plumbness specified in AISC 303 (AISC 2016d). For modeling purposes, an out-of-out straightness (camber) of $L/1{,}000$ was specified. Local web and flange imperfections expected during the manufacturing process are limited by ASTM (2014). Fig. 5(b) demonstrates the web and flange geometric imperfections implemented in the simulations.

A total of 110 wide-flange columns with sections selected from AISC (2016a) were analyzed to generate a comprehensive database. The sections ranged from W44 to W10 shapes and covered a wide range of slenderness parameters, as follows:

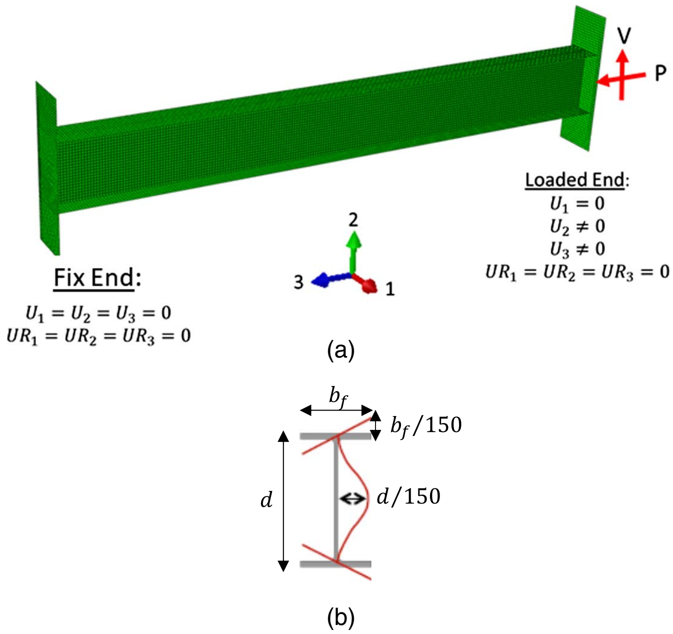

Fig. 5. Finite element model: (a) boundary conditions; and (b) section initial imperfections.

$$2.62 \leq \lambda_f \leq 10.2; \quad 5.66 \leq \lambda_w \leq 54.6; \quad 41.1 \leq \lambda_L \leq 120 \qquad (3)$$

Fig. 6 shows the distribution of the flange and web width-to-thickness ratios for the 110 specimens. Each fixed–fixed boundary condition model was cyclically loaded with the same AISC loading protocol used in the full-scale test with three levels of constant axial compressive force [$C_a = 0.2$, 0.4, and 0.6, where C_a is defined per Eq. (2)]. The yield stress of the steel was 379 MPa (55 Ksi). To evaluate the effect of yield stress on the behavior and to develop a compactness requirement that is a function of the yield stress, two additional yield stress levels, 345 MPa (50 Ksi) and 448 MPa (65 Ksi) with $C_a = 0.2$, were included in the analysis. Therefore, the database includes a total of 550 models. Fig. 7 shows representative results for several models, which demonstrate the predicted buckling mode and axial shortening of three W14 "shallow" columns. Depending on the λ_w value and the section depth-to-width ratio, d/b_f, a W14 column can buckle in one of the three buckling modes, and axial shortening can be significant.

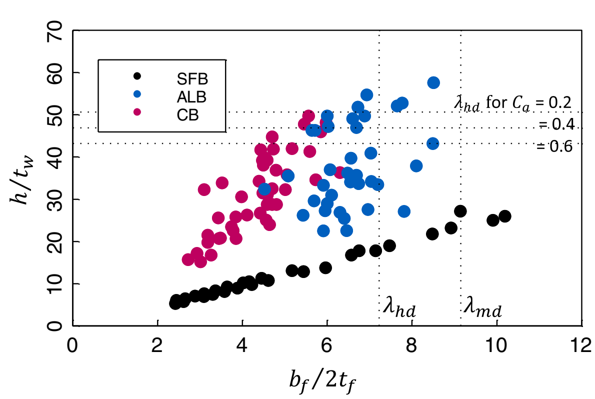

Fig. 6. Distribution of width-to-thickness ratios for finite element simulation.

Development of Web Compactness Limits for Seismic Design

Section compactness requirements in design standards for both nonseismic and seismic applications are generally established so the member can achieve a target plastic rotation capacity. In addition, flange local buckling and web local buckling are treated as separate limit states. Results from both testing and numerical simulations showed that wide-flange columns could experience significant flange and web local buckling under cyclic loading even when the cross section meets the highly ductile requirement for SMF design. It was observed that there is an interaction between web and flange local buckling that can trigger a significant degradation in the flexural strength and large axial shortening within the plastic hinge region. A procedure to establish seismic compactness requirements for webs to minimize this degradation is presented below.

Critical Story Drift Angle

The story drift angle (SDA) is the ratio of the lateral displacement of the top of the column to its length. Fig. 8(a) shows the typical cyclic response for a W24 × 176 column specimen with $C_a = 0.2$ and a fixed–fixed boundary condition that was subjected to the AISC loading sequence. The end moment, M, is normalized by an idealized reduced plastic moment, M_{pc}, that accounts for the axial load effect (ASCE-WRC 1971), as follows:

when $P/P_y \geq 0.15$

$$M_{pc} = 1.18\left(1 - \frac{P}{P_y}\right)M_p \qquad (4a)$$

when $P/P_y < 0.15$

$$M_{pc} = M_p \qquad (4b)$$

where M_p = plastic moment. Because the flexural strength degraded rapidly in the postbuckling region, it is difficult to define a limiting deformation (rotation) capacity. For beam-to-column connection qualification tests for use in an SMF, AISC 341 does not permit the flexural strength of the beam at the face of column to degrade below 80% of the nominal plastic moment of the beam at an SDA = 0.04 rad. This criterion is not adopted here for columns because it would be in the range where the column would experience excessive strength degradation, local and global buckling, and axial shortening in the plastic hinge. Also note, from Fig. 8(b), that axial shortening due to buckling increases rapidly once the section reaches its maximum flexural strength. Therefore, for column design, it is prudent to define a critical story drift angle, SDA_{cr}, as the lateral deformation capacity of the column beyond which significant flexural strength degradation is initiated [Fig. 8(a)].

Values of SDA_{cr} for the 550 numerically simulated columns and 22 tested columns, all with a fixed–fixed boundary condition, were first determined. A multivariate regression analysis was performed to fit the following model:

$$SDA_{cr} = C_0\lambda_w^{C_1}\left(1 - \frac{P_u}{P_{ya}}\right)^{C_2}\left(\frac{F_{ya}}{E}\right)^{(C_1/2)} \qquad (5)$$

where F_{ya} and P_{ya} = actual yield stress of the member and the associated yield strength of the column. Table 2 lists the measured F_{ya} values for both the flange and web of each test specimen. Considering the interactive nature of flange and web local buckling observed in this test program, for regression the F_{ya} value of each specimen was taken as the average value from the flange and web tensile coupon test results. Coefficients C_0, C_1, and C_2 remain to be determined from regression. Note that the exponent for the (F_{ya}/E)

J. Struct. Eng., 2021, 147(7): 04021100

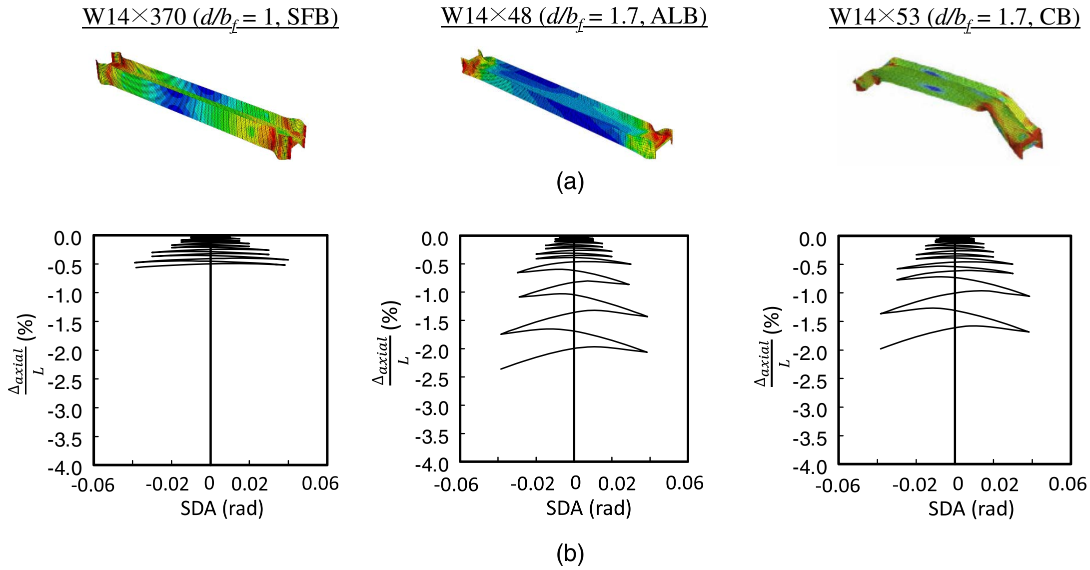

Fig. 7. W14 Sections with different buckling modes ($C_a = 0.2$): (a) buckling mode; and (b) axial shortening.

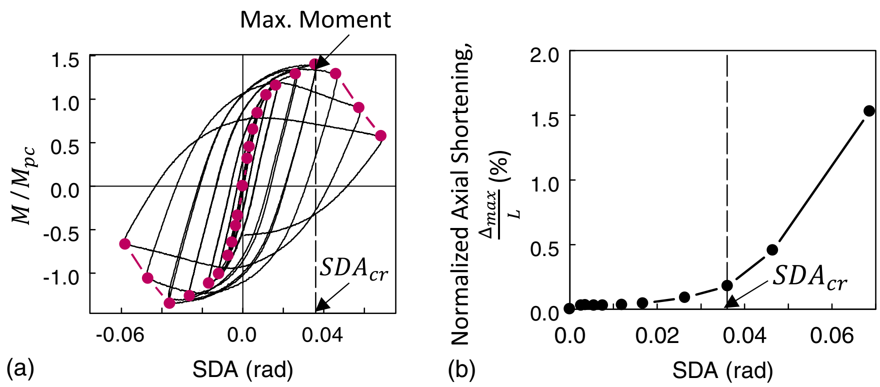

Fig. 8. Definition of critical story drift angle, SDA_{cr}: (a) cyclic response; and (b) axial shortening.

term is set equal to half that for the λ_w term so that the resulting λ_w expression can be expressed in the conventional form (Table 1) as a function of the square root of (F_{ya}/E). Also, λ_f was initially included in Eq. (5) but was found to be negligible and subsequently dropped because both λ_f and λ_w are correlated—that is, not statistically independent, for hot-rolled wide-flange sections listed in AISC (2016a). Considering the uncertainties associated with the assumptions made in the finite element simulation, it was decided to assign a larger weight (= 10) to each of the tested specimens than that (= 1) assigned to each of the simulated columns. The regression resulted in the following expression with a coefficient of determination, R^2, of 0.82

$$\mathrm{SDA}_{cr} = 4.949 \times 10^{-2} \lambda_w^{-0.929} \left(1 - \frac{P_u}{P_{ya}}\right)^{2.126} \left(\frac{F_{ya}}{E}\right)^{-0.465} \quad (6)$$

A comparison of the predicted and actual SDA_{cr} values of 572 data points is presented in Fig. 9.

Effective Critical Story Drift Angle

The critical story drift angle is affected by the boundary condition, loading protocol, and axial load type (constant or cyclical). Therefore, SDA_{cr} in Eq. (6) needs to be adjusted as follows to determine an effective critical story drift angle, SDA'_{cr}:

$$\mathrm{SDA}'_{cr} = \gamma \cdot \mathrm{SDA}_{cr} \quad (7)$$

where the adjustment factor γ has three components, as follows:

$$\gamma = \gamma_b \gamma_l \gamma_a \quad (8)$$

Factors γ_b, γ_l, and γ_a are used to account for the effects of changes in the boundary conditions, loading protocol, and axial load type, respectively.

Boundary Condition Factor, γ_b

Eq. (6) was developed for the fixed–fixed boundary condition as shown in Fig. 10(a). While the bottom end of the first-story columns in an SMF are usually designed to match this boundary condition and plastic hinge formation is expected, the top end of these columns would rotate due to the flexibility of connected beams [Fig. 10(b)]. To evaluate this effect, three pairs of specimens were tested with the fixed–fixed and fixed–rotating boundary conditions; the same constant axial load was applied to each pair of the specimens (Table 3). For example, Specimens 13M and 13M-BC were

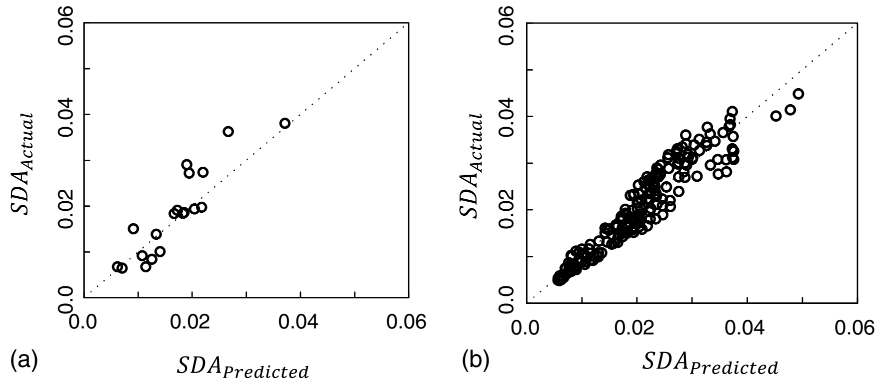

Fig. 9. Comparison of predicted and actual SDA_{cr} values: (a) test data; and (b) numerically simulated data.

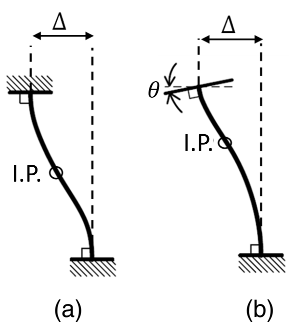

Fig. 10. Boundary conditions: (a) fixed–fixed case; and (b) fixed–rotating case.

Table 3. Boundary condition effect

Shape (C_a)	Specimen no.	SDA_{cr} (×0.01 rad)	$\frac{SDA_{cr}^{F-R}}{SDA_{cr}^{F-F}}$
W24 × 176 (0.6)	1H	1.37	1.31
	11H-BC	1.8	
W30 × 173 (0.4)	13M	0.81	1.60
	13M-BC	1.3	
W18 × 130 (0.4)	16M	2.8	1.32
	16M-BC	3.7	
			Average = 1.41

nominally identical; the only difference was that the boundary condition had a rotation imposed at one end of the column.

Based on results from nonlinear time-history analysis of a four-story SMF (Harris and Speicher 2015), it was assumed in testing that the rotating angle, θ, at one end (top end in an actual frame) was equal to the imposed story drift angle (also known as chord rotation in that study). This cyclic rotation was in phase with the cyclic story drift for testing.

Figs. 11 and 12 show a comparison of the buckling mode and hysteretic response (moment-rotation) of two pairs of specimens; the former one failed in CB and the latter failed in ALB. Having a rotating end at the top of the column would reduce the lateral stiffness of the story and the story drift angle would increase. However, this reduction did not change the buckling mode. To facilitate this comparison, the cyclic backbone curve of each specimen was first constructed (Fig. 13) based on the procedure defined in ASCE 41-17 (ASCE 2017). Specifically, the cyclic backbone curve is the envelope curve drawn through each point of peak drift during the first cycle of each increment of loading. Table 3 summarizes the values of SDA_{cr} as defined previously. The value for the fixed–rotating case (SDA_{cr}^{F-R}) is larger than that for the fixed–fixed case (SDA_{cr}^{F-F}). The average increase of SDA_{cr} is 41% for the three pairs of specimens, and, therefore, the value of γ_b is taken as 1.41.

Lateral Loading Sequence Factor, γ_l

Eq. (6) was developed with the AISC cyclic loading protocol [Fig. 3(a)], which features a symmetric cyclic loading sequence with increasing displacement amplitudes. It is well-known that loading pattern will affect the deformation capacity of a structural component; actual response of an SMF in a seismic event is not symmetric, and the response that leads to collapse tends to ratchet in one direction (Manson and Speicher 2016). Therefore, researchers have proposed alternative cyclic loading protocols for testing steel columns (e.g., Suzuki and Lignos 2014; Wu et al. 2018).

In the current study, the near-fault loading sequence [Fig. 3(b)] was used to evaluate the ratcheting effect. Two pairs of nominally identical specimens (Table 2) was used to evaluate the loading sequence effect. Figs. 14 and 15 show a comparison of the buckling modes and cyclic responses; the first pair failed in ALB and the latter in CB. For the specimens tested, it was observed that the loading sequence did not change the governing buckling mode.

Unlike that specified in ASCE 41 for the construction of the cyclic backbone curve, there is no established method to define a story drift capacity for responses with nonsymmetric loading. In determining the SDA_{cr}^{NF} values for the near-fault loading protocol, the origin was shifted from O to O′ as shown in Fig. 16; the value of SDA_{cr}^{NF} thus defined reflects the effect of the initial excursion to −0.02 rad [point "a" in Fig. 3(b)]. Once the values for both AISC loading protocol (SDA_{cr}^{AISC}) and near-fault loading protocol (SDA_{cr}^{NF}) were determined (Table 4), it was assumed that the ratcheting-type column response in an actual earthquake is bounded by these two values, an assumption which is similar to the actual response in a seismic event being bounded by the monotonic response curve and the cyclic backbone curve (NIST 2017). The actual SDA_{cr} is then taken as the average of the two. The ratio between this average value and SDA_{cr}^{AISC} is treated as γ_l, as follows:

$$\gamma_l = \frac{SDA_{cr}^{AISC} + SDA_{cr}^{NF}}{2(SDA_{cr}^{AISC})} \quad (9)$$

With the limited number of test data, the average value of γ_l is taken as 1.36.

J. Struct. Eng., 2021, 147(7): 04021100

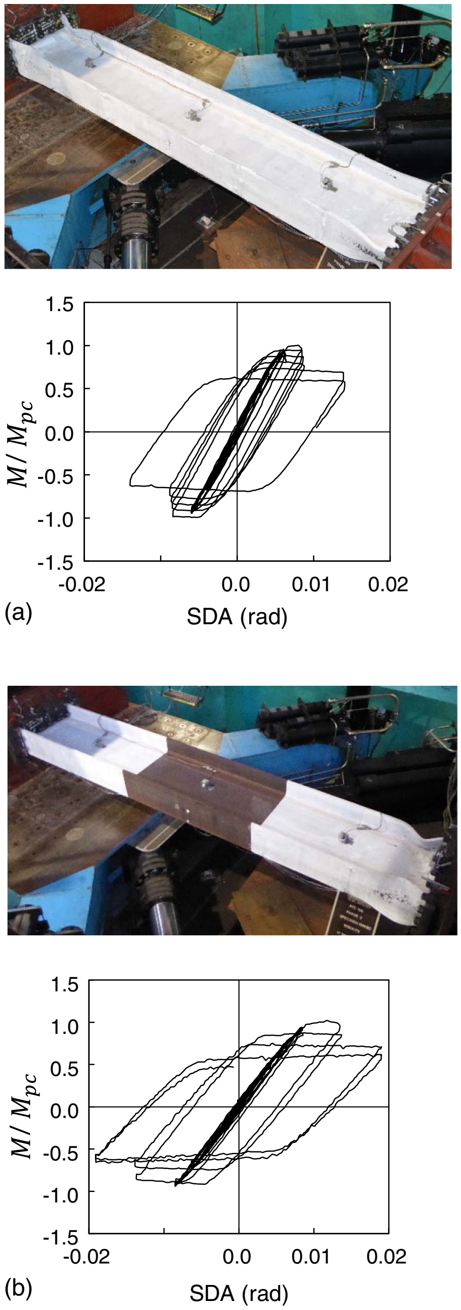

Fig. 11. Effect of end rotation boundary condition on W30 × 173 specimens: (a) fixed–fixed boundary (Specimen 13M); and (b) fixed–rotating boundary (Specimen 13M-BC).

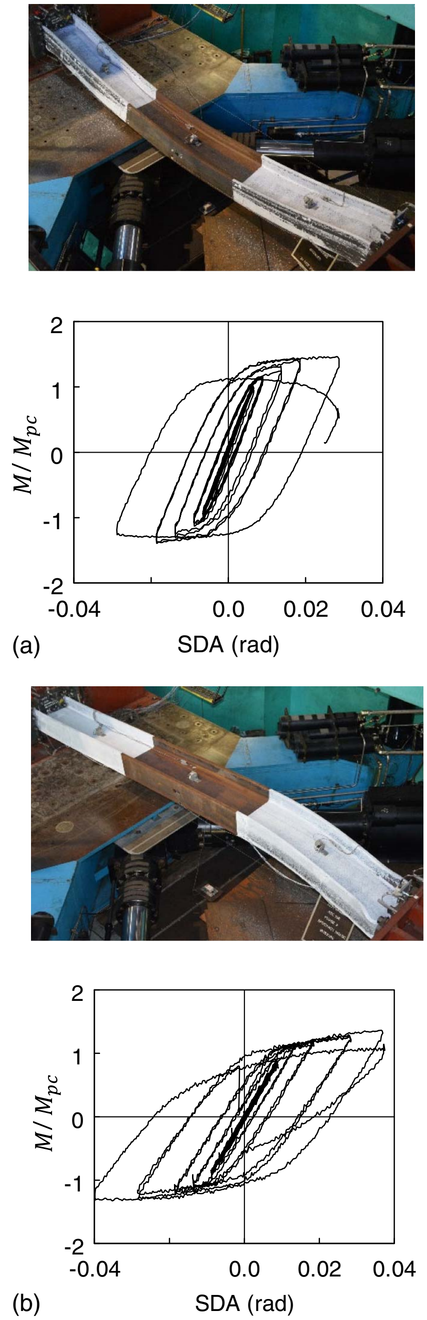

Fig. 12. Effect of end rotation boundary condition on W18 × 130 specimens: (a) fixed–fixed boundary (Specimen 16M); and (b) fixed–rotating boundary (Specimen 16M-BC).

Axial Loading Type Factor, γ_a

All specimens listed in Table 2 were tested with a constant axial load. These specimens are representative of interior frame columns in a multibay moment frame, where the axial load remains relatively constant during lateral motions. The axial load demand on the exterior frame columns will fluctuate due to the overturning moment effect. Therefore, four additional specimens (not included in Table 2) were tested with a cyclic axial load to simulate the demand on exterior columns (Chansuk et al. 2018). By applying the axial load cyclically with the imposed lateral drifts, test results (not shown here) showed that the maximum flexural strength would increase relative to a column loaded with a constant axial load. Local buckling and axial shortening were observed to be less severe. Therefore, the value of γ_a larger than 1.0 can be used to develop a limiting λ_w for highly and moderately ductile sections. The value of γ_a is taken as 1.0 for interior frame columns. The compactness requirement derived below with $\gamma_a = 1$ will be conservative when applied to exterior columns.

Proposed Limiting Web Slenderness Ratios

Based on data provided above, the value of γ equals

$$\gamma = \gamma_b \gamma_l \gamma_a = 1.41 \times 1.36 \times 1.0 = 1.92 \qquad (10)$$

Eq. (7) together with Eq. (10) then becomes

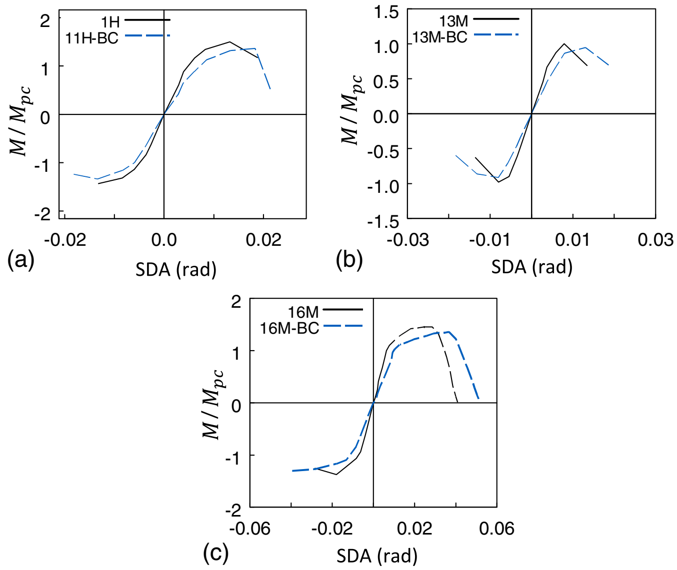

Fig. 13. Boundary condition effect: (a) W24 × 176 specimens; (b) W30 × 173 specimens; and (c) W18 × 130 specimens.

$$\mathrm{SDA}'_{cr} = 0.095\lambda_w^{-0.929}\left(1 - \frac{P_u}{P_{ya}}\right)^{2.126}\left(\frac{F_{ya}}{E}\right)^{-0.465} \tag{11}$$

Solving for λ_w in Eq. (11) gives the following expression:

$$\lambda_w = \frac{0.0794}{(\mathrm{SDA}'_{cr})^{1.08}}\left(1 - \frac{P_u}{P_{ya}}\right)^{2.29}\sqrt{\frac{E}{F_{ya}}} \tag{12}$$

For adoption in AISC 341, F_{ya} and P_{ya} can be replaced by the following, and C_a is redefined as in Eq. (13c):

$$F_{ya} = R_y F_y \tag{13a}$$

$$P_{ya} = R_y F_y A_g = R_y P_y \tag{13b}$$

$$C_a = \frac{P_u}{R_y F_y A_g} \tag{13c}$$

Note that Eq. (13c) does not contain ϕ_c in the denominator as in Eq. (2). Eq. (12) then becomes

$$\lambda_w = \frac{0.0794}{(\mathrm{SDA}'_{cr})^{1.08}}(1 - C_a)^{2.29}\sqrt{\frac{E}{R_y F_y}} \tag{14}$$

For SMF design, AISC 341 Section E3.6b requires beam-to-column moment connections to accommodate an SDA of at least 0.04 rad. Setting SDA'_{cr} in Eq. (14) to 0.04 rad, the resulting λ_w, which is defined as λ_{hd} for highly ductile members in AISC 341, becomes

$$\lambda_{hd} = 2.54(1 - C_a)^{2.29}\sqrt{\frac{E}{R_y F_y}} \tag{15}$$

Similarly, setting SDA'_{cr} to 0.02 rad for an IMF gives the limiting λ_{md} value for a moderately ductile section as

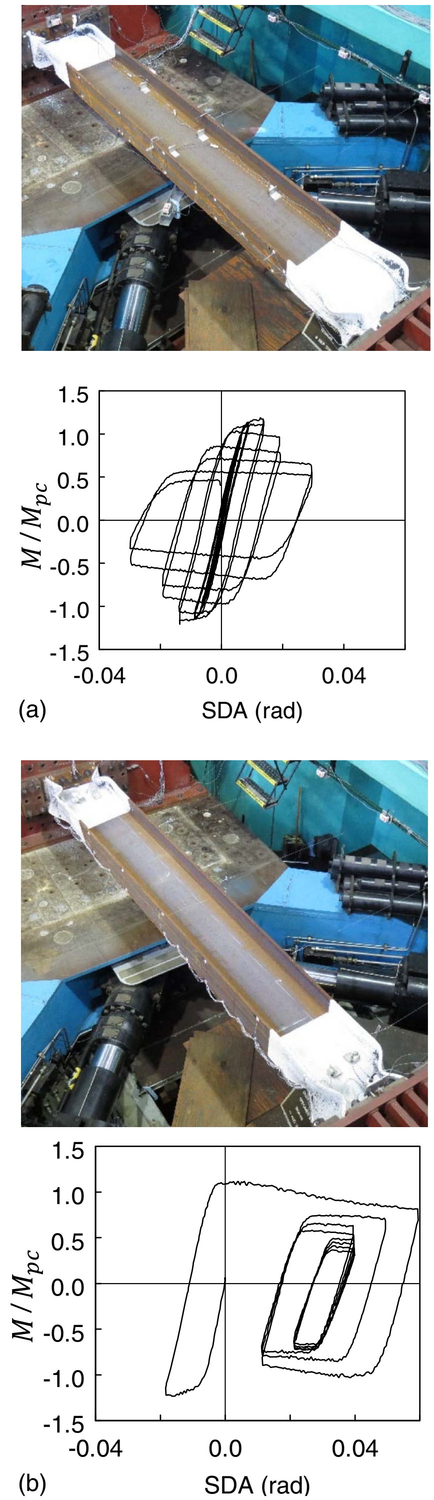

Fig. 14. Loading sequence effect on W24 × 131 specimens: (a) far-field loading (Specimen 2M); and (b) near-field loading (Specimen 2M-NF).

$$\lambda_{md} = 5.35(1 - C_a)^{2.29}\sqrt{\frac{E}{R_y F_y}} \tag{16}$$

Fig. 17 compares the proposed web slenderness limit with those currently specified in AISC 341-16. The proposed equations can be rounded to the following expressions without loss of accuracy:

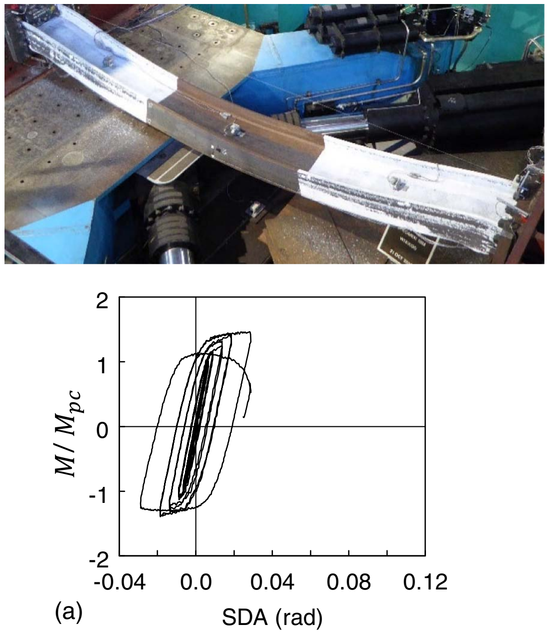

Fig. 15. Loading sequence effect on W18 × 130 specimens: (a) far-field loading (16M); and (b) near-field loading (21M-NF).

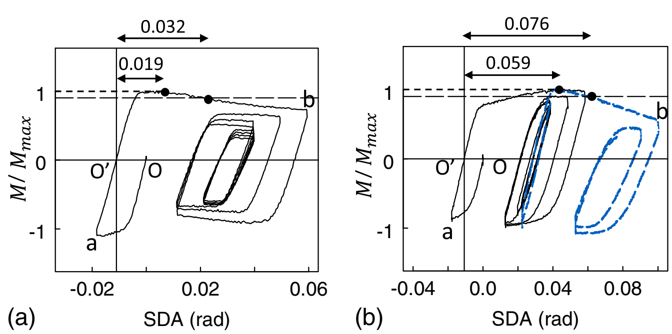

Fig. 16. Determination of SDA_{cr} for near-fault loading response: (a) Specimen 2M-NF; and (b) Specimen 21M-NF.

Table 4. Lateral loading protocol effect

Shape (C_a)	Specimen no.	SDA_{cr} ($\times 0.01$ rad)	Eq. (9)
W24 × 131 (0.4)	2M	1.35	1.20
	2M-NF	1.89	
W18 × 130 (0.4)	16M	2.88	1.52
	21M-NF	5.9	
			Average = 1.36

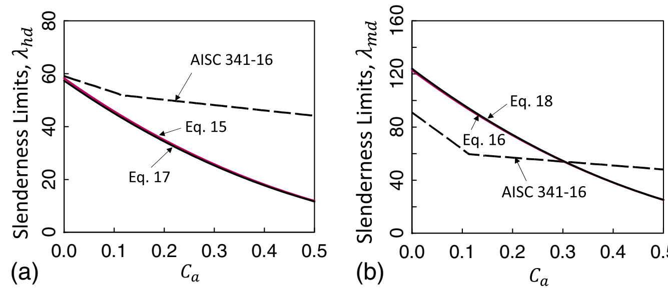

Fig. 17. Comparison of proposed and AISC 341 web slenderness limits (ASTM A992 steel): (a) SMF; and (b) IMF.

$$\lambda_{hd} = 2.54(1 - C_a)^{2.29}\sqrt{\frac{E}{R_y F_y}} \approx 2.5(1 - C_a)^{2.3}\sqrt{\frac{E}{R_y F_y}} \quad (17)$$

$$\lambda_{md} = 5.35(1 - C_a)^{2.29}\sqrt{\frac{E}{R_y F_y}} \approx 5.4(1 - C_a)^{2.3}\sqrt{\frac{E}{R_y F_y}} \quad (18)$$

Limitations of Proposed Web Slenderness Limits

The above limiting web slenderness ratios should be applied with the limiting flange slenderness ratios specified in AISC 341 and with restrictions. To ensure adequate ductility in columns developing plastic hinges, plastic design provisions require that the design strength in compression not exceed $0.75P_y$ per AISC 360 (2016c). This plastic analysis requirement does not capture the cyclic loading effect. It is suggested that the C_a value be limited to 0.5, a value similar to that specified in ASCE 41-17 (ASCE 2017) to distinguish between columns permitted to yield in flexure. ASCE 41-17 maintains a cap on the axial compression of 0.75 times the expected yield strength, R_yP_y, for stability.

Note that the fixed–fixed boundary condition provides a more critical, and hence conservative, condition for establishing the upper bound value for L/r_y, beyond which the susceptibility of global buckling is increased. Both testing and numerical simulations conducted in this research with fixed–fixed boundary condition showed that the L/r_y ratio did not significantly affect the column cyclic response as long as it was not higher than 120. Given that AISC 341 does not provide a limiting L/r_y value for columns expected to develop plastic hinges from lateral story drifts, it is suggested that L/r_y be limited to 120.

Summary and Conclusions

This study comprised testing and numerical simulation of deep, slender, wide-flange steel columns subject to cyclic lateral drifts and axial compression. It was found that significant local buckling triggers a rapid degradation in flexural strength. The much larger width-to-thickness ratio of the web in the deep columns was not effective in restraining and delaying local buckling of the flanges, as was observed in the shallow, stocky columns (e.g., W12 or W14). The flexural strength of deep columns degraded rapidly because of the interaction between flange and web local buckling. This interaction was accompanied by significant axial shortening in the plastic hinge region. In addition, the larger L/r_y of deep columns also triggered out-of-plane buckling.

Based on the results from both testing and numerical simulation, a critical story drift angle, SDA_{cr}, at which point significant flexural strength degradation and axial shortening would initiate, was first established [Eq. (6)]. SDA_{cr} was then adjusted to account for the effects of changes in the boundary condition and lateral loading sequence to determine an effective critical story drift angle, SDA'_{cr} [Eq. (11)]. Setting this effective deformation capacity of the column to the target values specified in AISC 341 (0.04 rad for SMF and 0.02 rad for IMF), enhanced web slenderness limits to prevent severe axial shortening were proposed for both highly ductile [Eq. (17)] and moderately ductile [Eq. (18)] sections.

Data Availability Statement

Some or all data, models, or code that support the findings of this study are available from the corresponding author upon reasonable request. This includes the test data. In addition, all test videos have been posted on YouTube.

Acknowledgments

Funding for this research was provided by the Applied Technology Council under its Earthquake and Structural Engineering Research contract with the National Institute of Standards and Technology. Mr. J. O. Malley (Degenkolb Engineers) chaired the Project Advisory Committee. Mrs. A. Hortacsu (Applied Technology Council) served as the Project Manager. The authors would like to acknowledge the American Institute of Steel Construction for providing steel materials and The Herrick Corporation for providing fabrication of the test specimens.

References

AISC. 2010. *Seismic provisions for structural steel buildings*. ANSI/AISC 341-10. Chicago: AISC.

AISC. 2016a. *Manual of steel construction*. Chicago: AISC.

AISC. 2016b. *Seismic provisions for structural steel buildings*. ANSI/AISC 341-16. Chicago: AISC.

AISC. 2016c. *Specification for structural steel buildings*. ANSI/AISC 360. Chicago: AISC.

AISC. 2016d. *Code of standard practice for steel buildings and bridges*. ANSI/AISC 303. Chicago: AISC.

ASCE. 2017. *Seismic evaluation and rehabilitation of existing buildings*. ASCE/SEI 41-17. Reston, VA: ASCE.

ASCE-WRC (Welding Research Council). 1971. *Plastic design in steel: A guide and commentary.* New York: WRC.

ASTM. 2014. *Standard specification for general requirements for rolled structural steel bars, plates, shapes, and sheet piling*. ASTM A6/A6M-14. West Conshohocken, PA: ASTM.

ASTM. 2015. *Standard specification for structural steel shapes*. ASTM A992/A992M-11. West Conshohocken, PA: ASTM.

Chansuk, P., G. Ozkula, and C.-M. Uang. 2018. *Seismic behavior and design of deep, slender wide-flange structural steel beam-columns: Phase 2 testing*. Rep. No. SSRP-18/02. San Diego: Univ. of California.

Chi, B., and C.-M. Uang. 2006. "Cyclic response and design recommendations of reduced beam section moment connections with deep columns." *J. Struct. Eng.* 132 (3): 346–357. https://doi.org/10.1061/(ASCE)0733-9445(2006)132:3(346).

Cravero, J., A. Elkady, and D. G. Lignos. 2020. "Experimental evaluation and numerical modeling of wide-flange steel columns subjected to constant and variable axial load coupled with lateral drift demands." *J. Struct. Eng.* 146 (3): 04019222. https://doi.org/10.1061/(ASCE)ST.1943-541X.0002499.

Elkady, A., and D. G. Lignos. 2012. "Dynamic stability of deep slender steel columns as part of special MRSF designed in seismic regions: Finite element modelling." In *Proc., 1st Int. Conf. on Performance-Based and Life-Cycle Structural Engineering*. Hong Kong: Hong Kong Polytechnic Univ.

Elkady, A., and D. G. Lignos. 2015. "Analytical investigation of the cyclic behavior and plastic hinge formation in deep wide-flange steel beam-columns." *Bull. Earthquake Eng.* 13 (4): 1097–1118. https://doi.org/10.1007/s10518-014-9640-y.

Elkady, A., and D. G. Lignos. 2018. "Full-scale testing of deep wide-flange steel columns under multi-axis cyclic loading: Loading sequence, boundary effects and out-of-plane brace force demands." *J. Struct. Eng.* 144 (2): 04017189. https://doi.org/10.1061/(ASCE)ST.1943-541X.0001937.

FEMA. 1997. *NEHRP guidelines for the seismic rehabilitation of buildings*. FEMA-273. Washington, DC: FEMA.

FEMA. 2000. *Recommended seismic design criteria for new steel moment-frame buildings*. FEMA-355A. Washington, DC: FEMA.

Fogarty, J., and S. El-Tawil. 2015. "Collapse resistance of steel columns under combined axial and lateral loading." *J. Struct. Eng.* 142 (1): 04015091. https://doi.org/10.1061/(ASCE)ST.1943-541X.0001350.

Fogarty, J., T. Y. Wu, and S. El-Tawil. 2017. "Collapse response and design of deep steel columns subjected to lateral displacement." *J. Struct. Eng.* 143 (9): 04017130. https://doi.org/10.1061/(ASCE)ST.1943-541X.0001848.

Harris, J. L., and M. S. Speicher. 2015. *Assessment of first generation performance-based seismic design methods for new steel buildings, Volume 1: Special moment frames*. Gaithersburg, MD: NIST.

Inamasu, H., A. M. Kanvinde, and D. G. Lignos. 2019. "Seismic stability of wide-flange steel columns interacting with embedded column base connections." *J. Struct. Eng.* 145 (12): 04019151. https://doi.org/10.1061/(ASCE)ST.1943-541X.0002410.

Krawinkler, H., A. Gupta, R. Medina, and N. Luco. 2000. *Loading histories for seismic performance testing of SMRF components and assemblies*. Rep. No. SAC/BD-00/10. Sacramento, CA: SAC Joint Venture California.

MacRae, G. 1990. *The seismic response of steel frames*. Rep. No. 90-6. Christchurch, New Zealand: Univ. of Canterbury.

Manson, B., and M. S. Speicher. 2016. "Loading protocols for ASCE 41 backbone curves." *Earthquake Spectra* 32 (4): 2513–2532.

Newell, J. D., and C-M. Uang. 2006. *Cyclic behavior of steel columns with combined high axial load and drift demand*. Rep. No. SSRP-06/22. San Diego: Univ. of California.

Newell, J. D., and C.-M. Uang. 2008. "Cyclic behavior of steel wide-flange columns subjected to large drift." *J. Struct. Eng.* 134 (8): 1334–1342. https://doi.org/10.1061/(ASCE)0733-9445(2008)134:8(1334).

NIST. 2011. *Research plan for the study of seismic behavior and design of deep, slender, wide-flange structural steel-beam-column members*. NIST-GCR-11-917-13. Gaithersburg, MD: NIST.

NIST. 2017. *Guidelines for nonlinear structural analysis and design of buildings, Part I–general*. NIST-GCR-17-917-46. Gaithersburg, MD: NIST.

Ozkula, G., J. Harris, and C.-M. Uang. 2017. "Classifying cyclic buckling modes of steel wide-flange columns under cyclic loading." In *Structures congress*, 155–167. Reston, VA: ASCE.

Ozkula, G., and C.-M. Uang. 2015. *Seismic behavior and design of deep, slender wide-flange structural steel beam-column members: Phase 1*. Rep. No. SSRP-15/06. San Diego: Univ. of California.

Popov, E. P., V. V. Bertero, and S. Chandramoulli. 1975. *Hysteretic behavior of steel columns*. Rep. No. UCB/EERC 75-11. Richmond, VA: Earthquake Engineering Research Center.

Schneider, S. P., C. W. Roeder, and J. E. Carpenter. 1993. "Seismic behavior of moment-resisting steel frames: Experimental study." *J. Struct. Eng.* 119 (6): 1885–1902. https://doi.org/10.1061/(ASCE)0733-9445(1993)119:6(1885).

Suzuki, Y., and D. G. Lignos. 2014. "Development of loading protocols for experimental testing of steel columns subjected to combined high axial load and lateral drift demands near collapse." In *Proc., 10th National Conf. on Earthquake Engineering*. Oakland, CA: Earthquake Engineering Research Institute.

Wu, T. Y., S. El-Tawil, and J. McCormick. 2018. "Highly ductile limits for deep steel columns." *J. Struct. Eng.* 144 (4): 04018016. https://doi.org/10.1061/(ASCE)ST.1943-541X.0002002.

Zargar, S., R. A. Medina, and E. Miranda. 2014. "Cyclic behavior of deep steel columns subjected to large deformation demands and high axial loads." In *Proc., 10th U.S. National Conf. on Earthquake Engineering*. Oakland, CA: Earthquake Engineering Research Institute.